

Local Model Explanations and Uncertainty Without Model Access

Surin Ahn* Justin Grana† Yafet Tamene‡ Kristian Holsheimer§

Abstract

We present a model-agnostic algorithm for generating post-hoc explanations and uncertainty intervals for a machine learning model when only a sample of inputs and outputs from the model is available, rather than direct access to the model itself. This situation may arise when model evaluations are expensive; when privacy, security and bandwidth constraints are imposed; or when there is a need for real-time, on-device explanations. Our algorithm constructs explanations using local polynomial regression and quantifies the uncertainty of the explanations using a bootstrapping approach. Through a simulation study, we show that the uncertainty intervals generated by our algorithm exhibit a favorable trade-off between interval width and coverage probability compared to the naive confidence intervals from classical regression analysis. We further demonstrate the capabilities of our method by applying it to black-box models trained on two real datasets.

1 Introduction

The advent and deployment of machine learning (ML) and artificial intelligence (AI) systems across numerous sectors have elevated the need to understand and explain such systems. Transparency and explainability of ML models are critical for debugging their mistakes, investigating their bias and fairness [36], building user trust in their decision-making, and in general making them more “human-centric” [26]. For example, explainability is crucial when determining why a malware classifier missed malicious content [18], examining errors in the behavior of an autonomous vehicle [15], or conveying to a person why their loan application was rejected [9, 19]. The profound societal implications of deploying “black-box” systems have spurred regulations such as the European Union’s General Data Protection Regulation (GDPR), which purportedly establishes explanations of algorithmic decision making as a fundamental human right [16]. Recently, the White House released a blueprint for an “AI Bill of Rights”, outlining a plan for enforcing the accountability, explainability and trustworthiness of AI systems [33].

The demand for model explainability has given rise to several methods that provide practitioners with insights into the key drivers of an ML model. While some methods take the approach of replacing black-box models with flexible, human-interpretable models [24], others such as LIME [25] and SHAP [22] focus on constructing post-hoc explanations of black-box models. Given the technical and societal importance of model explainability, it is no surprise that additional remedies continue to arise (see surveys [37, 23, 20, 1, 11]). Furthermore, the potential applications of model explainability are expanding rapidly, ranging from professional sports predictions [28] to cancer diagnosis [17].

A major limitation of current methods is that they require direct access to the underlying model (i.e., the ability to query the model arbitrarily, in real-time) to construct explanations. For example, LIME and SHAP estimate the importance of each feature on the prediction by observing the model outputs under numerous local perturbations of the input instance. However, there are many situations in which model access is restricted or entirely unavailable. Some inhibiting factors—all of which are especially prevalent in production-grade systems—include the complexity of the engineering pipeline, model privacy and security concerns, and the need for real time, on-device explanations. Instead, it is often more feasible to collect a batch of input-output samples from the model in advance and use this fixed dataset to construct explanations.

*Stanford University. surinahn@stanford.edu. Work completed during an internship at Microsoft.

†Edge & Node. justin@edgeandnode.com. Work completed while a full-time employee at Microsoft.

‡Microsoft. yafettamene@microsoft.com

§DeepMind. holsheimer@google.com. Work completed while a full-time employee at Microsoft.

Motivated by this problem, we introduce a new method to: (i) build local model-agnostic explanations from a historical dataset of model inputs and outputs, without the need for direct model access; and (ii) quantify the uncertainty associated with the explanations.

The first objective is achieved by performing local polynomial regression on the set of points in the dataset closest to the input instance, and then extracting feature importance scores from the resulting polynomial surrogate model. The second objective is achieved using a non-parametric technique from statistics known as *bootstrapping* [13] to provide a measure of uncertainty in the feature importance scores. Providing uncertainty measures is crucial due to the inevitable loss of precision from using a fixed dataset to generate explanations. While quantifying uncertainty is important for any explainer, it is especially important when model access is unavailable since one cannot arbitrarily query the model to obtain higher-fidelity explanations.

Our main motivation for employing a non-parametric bootstrap technique is that the uncertainty in our explanations does not stem from the same type of sampling error found in traditional statistical models. Thus, adopting parametric statistical methods can generate misleading results. Broadly speaking, the error in traditional regression models comes from the stochastic nature of both the random sample of inputs as well as the response for a fixed input. Often, inference is conducted under the assumption that the data generating process is correctly specified (e.g., a generalized linear model). In our setting, explanations are still subject to the randomness of the input sample (i.e., the points included in the fixed dataset); but for a fixed input, the response (i.e., the output of the ML model) is deterministic.¹ We do not assume that our surrogate model correctly specifies the underlying ML model, and thus our explanations incur error due to *model misspecification* (sometimes called “model credibility” [38]). Consequently, since the assumption of correct model specification in traditional parametric statistics does not apply in this environment, we would expect a non-parametric uncertainty interval to perform more favorably than its parametric counterparts.

Related Work While our work is unique in that we do not assume access to the underlying ML model, our approach builds upon previous methods that attempt to quantify the uncertainty of explanations. These include methods that apply standard sampling error techniques to explainability [30] as well as non-parametric approaches [27, 35]. While [27] also employs bootstrap methods, our approach is different in that we focus on gradient estimation of the ML model instead of rank orders of feature importance. Additionally, [35] focuses on quantifying the uncertainty in explanations of convolutional neural networks, while our method is model-agnostic.

Finally, our work is tangentially related to the stability of ML model explanations [4, 3, 2]. This research thrust examines the sensitivity of explanations to perturbations of the input data. Although in the environment we consider it is impossible to observe the model outputs under arbitrary input perturbations, our bootstrap resampling method still allows us to quantify the sensitivity of explanations from a fixed dataset. It does so by aggregating explanations computed from several local subsets of the data (i.e., input samples generated from the empirical distribution of the fixed dataset).

Contributions We introduce a novel method for constructing local model-agnostic explanations from a fixed dataset of inputs and outputs from the underlying model. In addition to generating point estimates of the feature importance scores, we provide a measure of uncertainty in these estimates using a non-parametric bootstrapping approach. We demonstrate the efficacy of our method through a simulation study. Specifically, we provide evidence that our bootstrapped uncertainty intervals Pareto-dominate the naive frequentist confidence intervals from classical regression analysis. We also provide evidence that our method is more practical than an existing Bayesian approach [30] in an environment without model access. Finally, we further demonstrate the capabilities of our method by applying it to black-box classification models trained on the COMPAS recidivism [6] and German Credit datasets from the UCI repository [12].

¹We do not consider ML models with stochastic outputs, such as many generative models.

2 Methodology

Setup Let $f : \mathbb{R}^d \rightarrow \mathbb{R}$ denote a black-box ML model which maps a d -dimensional feature vector to some prediction.² In classification tasks, $f(x) \in [0, 1]$ represents the probability that x belongs to a particular class. Instead of direct access to f , we are given a fixed dataset of n input-output pairs from the model: $\mathcal{D} \triangleq \{(x^{(i)}, f(x^{(i)}))\}_{i=1}^n$. Let $x^* \in \mathbb{R}^d$ be the input instance whose model prediction, $f(x^*)$, we would like to explain, and let $\pi_{x^*} : \mathbb{R}^d \rightarrow \mathbb{R}_+$ be a *proximity function* which provides a measure of closeness to x^* . For example, LIME [25] uses an exponential kernel applied to the ℓ_2 distance.

Feature Importance Definition Given \mathcal{D} , our objective is two-fold. First, we would like to estimate the *feature importance scores*, i.e., the influence of each feature on the model prediction. For simplicity and concreteness, and to ensure the availability of a “ground truth” in our experiments, we focus on estimating *gradients* and *local function differences*, which are commonly used proxies for feature importance [7, 29, 32, 31, 5]. The gradient of f at x^* is denoted by $\nabla_x f(x^*)$ and defined as:

$$\nabla_x f(x^*) \triangleq \left[\frac{\partial f}{\partial x_1}(x^*) \quad \frac{\partial f}{\partial x_2}(x^*) \quad \dots \quad \frac{\partial f}{\partial x_d}(x^*) \right]^\top.$$

Intuitively, if $\left| \frac{\partial f}{\partial x_j}(x^*) \right|$ is large, then a small change in the j^{th} feature results in a large change in the model output, suggesting that the feature played a non-trivial role in the prediction. Note that when f is a linear model, i.e., $f(x) = \beta_0 + \beta^\top x$ for some $\beta \in \mathbb{R}^d$, the gradient is simply the vector of coefficients β .

In certain situations (e.g., when features are categorical or ordinal, the model is non-differentiable, or the gradient is not a suitable measure of feature importance³), it is useful to estimate the local function differences instead of the instantaneous partial derivatives. If the j^{th} feature is continuous or ordinal, we define the function difference around x^* with respect to the j^{th} feature to be

$$f(x_+^*) - f(x_-^*),$$

where x_+^* (resp. x_-^*) is equal to x^* with the j^{th} entry set to $x_j^* + \delta$ (resp. $x_j^* - \delta$), and δ is a domain-specific parameter specified by the user or set to some default constant that captures a “one-unit change” in that feature (e.g., a value proportional to the standard deviation). For categorical features, we seek to estimate $f(x^*) - f(x_{\text{base}}^*)$, where x_{base}^* is x^* with the j^{th} entry set to a baseline or counterfactual category, which can be domain-specific or based on the relative frequencies of the categories in the dataset. This represents the amount that f changes, *ceteris paribus*, when the j^{th} feature is switched from its baseline category to the current category x_j^* .

Uncertainty Intervals Our second goal is to construct something analogous to a *confidence interval* $\mathcal{C} \subset \mathbb{R}$, indicating the level of uncertainty in our point estimate. A confidence interval at confidence level $100 \cdot (1 - \alpha)\%$ is an interval for which $100 \cdot (1 - \alpha)\%$ of the intervals constructed from repeated samples contain the true parameter of interest (in our case, the partial derivatives or function differences of f with respect to each feature). The most common value of α is 0.05, resulting in a confidence level of 95%.

We will refer to the estimated uncertainty around our explanations as “uncertainty intervals” rather than “confidence intervals”. We make this distinction to re-enforce that our uncertainty measures do not correspond to the frequentist definition of a confidence interval. This is once again due to the violated assumption of correct model specification. It is known that model misspecification can either increase or decrease the power of a statistical test [21], and that correcting for the misspecification is often a problem-specific task [34, 8]. Thus, we cannot compare the coverage probability of our bootstrap intervals with a pre-specified significance level (as is typically done in frequentist statistics). Instead, we will characterize the efficacy of our method by examining the *trade-off*—in the form of a “Pareto frontier”—between the coverage probability and interval width.

²Though we focus on models that produce a scalar output, our methods can be straightforwardly extended to the case of vector outputs (e.g., a softmax layer for multiclass classification).

³Consider an ML model that exhibits step function-like behavior. Such models are not amenable to gradient-based explainability since the instantaneous derivatives are zero almost everywhere.

Algorithm 1 Estimating feature importance scores via local polynomial regression

- 1: **Input:** Instance $x^* \in \mathbb{R}^d$, dataset \mathcal{D} , polynomial degree k , neighborhood size m , proximity function $\pi_{x^*}(\cdot)$
 - 2: **Initialize:** $Z \in \mathbb{R}^d$
 - 3: $\mathcal{N}_{x^*} \leftarrow m$ closest points to x^* in \mathcal{D} according to $\pi_{x^*}(\cdot)$
 - 4: $y \leftarrow$ labels of points in \mathcal{N}_{x^*} , taken from \mathcal{D}
 - 5: $X \leftarrow$ design matrix of points in \mathcal{N}_{x^*} , transformed to polynomial features of degree k with interaction terms
 - 6: $\hat{\beta} \leftarrow (X^\top X)^{-1} X^\top y$
 - 7: $g \leftarrow$ degree- k polynomial with interaction terms, parameterized by $\hat{\beta}$
 - 8: **for** $j = 1$ to d **do**
 - 9: **if** feature j is continuous **then**
 - 10: $Z_j \leftarrow \frac{\partial g}{\partial x_j}(x^*)$ or $g(x_+^*) - g(x_-^*)$
 - 11: **else if** feature j is categorical **then**
 - 12: $Z_j \leftarrow g(x^*) - g(x_{\text{base}}^*)$
 - 13: **end if**
 - 14: **end for**
 - 15: **return** Z
-

3 Algorithms

We now describe our algorithms for generating local explanations with uncertainty quantification, given only a fixed dataset of input-output pairs from the model. To generate the explanation itself, we fit a low-degree polynomial g to the points in the dataset most similar to x^* , then return the partial derivatives or local function differences of g with respect to each feature. The intuition is that even if f is globally nonlinear, it can be sufficiently well-approximated by a low-degree polynomial in the vicinity of x^* . To quantify the uncertainty in the explanation, we perform a bootstrapping procedure in which we repeatedly obtain explanations from sub-samples of the neighborhood around x^* , then return the percentiles of the resulting bootstrap distribution corresponding to the desired confidence level.

Estimating Feature Importance Our approach to estimating the local feature importance scores of f around x^* is outlined in Algorithm 1 and—at a high level—can be summarized as follows:

1. Within the dataset \mathcal{D} , identify the m points closest to x^* according to the chosen proximity function $\pi_{x^*}(\cdot)$. Denote this neighborhood around x^* by \mathcal{N}_{x^*} .
2. Fit a degree- k polynomial, g , to the local dataset $\{(z, f(z)) : z \in \mathcal{N}_{x^*}\} \subseteq \mathcal{D}$.
3. Return the partial derivative or local function differences of g with respect to each feature, evaluated at the query point x^* .

The primary hyperparameters of our algorithm are m —which controls the size of the neighborhood around x^* —and k —which is the degree of the local polynomial fit to the neighborhood. There is a trade-off associated with each hyperparameter. Increasing m provides more data for the regression but may diminish the quality of the estimate by including points that are further away from x^* and hence less relevant to its local explanation. A “middle ground” can be achieved by performing weighted regression in Step 2 above, with weights given by $\{\pi'_{x^*}(z) : z \in \mathcal{N}_{x^*}\}$, where $\pi'_{x^*}(\cdot)$ is some proximity function (not necessarily the same as $\pi_{x^*}(\cdot)$). In general, m should scale with the “density” of the dataset \mathcal{D} in the vicinity of x^* , since a higher density means there are more points similar to x^* that can potentially aid the explanation. If the goal is to estimate function differences, the neighborhood size should also take into account the δ values for each continuous feature. Similarly, a larger k allows for a more expressive model (and potentially a better local approximation to f) but at the cost of requiring a larger m .⁴ In most instances, we found $k \leq 4$ to yield good performance. We discuss further strategies for selecting the hyperparameters in Section 4.3.

⁴Recall that $k + 1$ points uniquely determine a polynomial of degree k .

Algorithm 2 Constructing bootstrap uncertainty intervals

```
1: Input: Instance  $x^* \in \mathbb{R}^d$ , dataset  $\mathcal{D}$ , polynomial degree  $k$ , neighborhood size  $m$ , number of bootstrap
   samples  $B$ , bootstrap neighborhood proportion  $c$ , significance level  $\alpha \in [0, 1]$ 
2: Initialize:  $Z \in \mathbb{R}^{B \times d}$ 
3:  $\mathcal{N}_{x^*} \leftarrow m$  closest points to  $x^*$  in  $\mathcal{D}$  according to  $\pi_{x^*}(\cdot)$ 
4: for  $i = 1$  to  $B$  do
5:    $\mathcal{N}'_{x^*} \leftarrow \lfloor cm \rfloor$  points sampled uniformly from  $\mathcal{N}_{x^*}$ 
6:    $y \leftarrow$  labels of points in  $\mathcal{N}'_{x^*}$ , taken from  $\mathcal{D}$ 
7:    $X \leftarrow$  design matrix of points in  $\mathcal{N}'_{x^*}$ , transformed to polynomial features of degree  $k$  with interaction
   terms
8:    $\hat{\beta} \leftarrow (X^\top X)^{-1} X^\top y$ 
9:    $g \leftarrow$  degree- $k$  polynomial with interaction terms, parameterized by  $\hat{\beta}$ 
10:  for  $j = 1$  to  $d$  do
11:    if feature  $j$  is continuous then
12:       $Z_{ij} \leftarrow \frac{\partial g}{\partial x_j}(x^*)$  or  $g(x_+^*) - g(x_-^*)$ 
13:    else if feature  $j$  is categorical then
14:       $Z_{ij} \leftarrow g(x^*) - g(x_{\text{base}}^*)$ 
15:    end if
16:  end for
17: end for
18: for  $j = 1$  to  $d$  do
19:    $L_j \leftarrow (100 \cdot \frac{\alpha}{2})^{\text{th}}$  percentile of  $Z_{:,j}$ 
20:    $U_j \leftarrow (100 \cdot (1 - \frac{\alpha}{2}))^{\text{th}}$  percentile of  $Z_{:,j}$ 
21: end for
22: return  $[L_j, U_j]$  for each  $j \in [d]$ 
```

Comparison with LIME Algorithm 1 is similar to LIME in the sense that a simple, interpretable model is fit to a set of points close to x^* . However, LIME makes two fundamental assumptions which differ from ours. First, it assumes one has direct access to the model. Second, it assumes the model is locally linear around x^* . Under these assumptions, LIME estimates feature importance by querying the model at samples (perturbations) that are arbitrarily close to x^* and fitting a sparse linear model to the resulting local dataset.

In our setting, however, we cannot query the model at arbitrary perturbations of x^* . Instead, we only have access to the fixed dataset \mathcal{D} , whose points may not be sufficiently close to x^* for a linear model to be a suitable local approximation to f . To mitigate this, we allow for an expanded class of interpretable models, including not just linear models but also higher-order polynomials with interaction terms. Intuitively, even if the points in \mathcal{D} are relatively far from x^* , using a more expressive model allows us to locally approximate the true underlying model with higher fidelity and obtain more accurate feature importance estimates as a result.

We also note that our approach to generating explanations with uncertainty intervals (see below) can be used in a “plug-and-play” fashion with any local interpretable model (e.g., decision trees), not just polynomials. However, we focus on polynomial models in this paper because they are differentiable and allow us to derive theoretical confidence intervals to use as a baseline in our simulation study (see Section 4.1).

Bootstrap Uncertainty Intervals The *bootstrap* [13] is a well-known resampling method for estimating the sampling distribution of any statistic. It is particularly useful when the sampling distribution is unknown, which is the case in our setting. Our high-level approach is to repeatedly perform the previously described local regression procedure on *sub-samples* of the neighborhood around x^* to build a bootstrap distribution of feature importance scores, from which we derive our uncertainty intervals. Our algorithm computes the *percentile bootstrap* [14], though we note that there are many alternative methods for constructing confidence intervals from the bootstrap distribution. The details are provided in Algorithm 2 and can be summarized as follows:

0. As before, let \mathcal{N}_{x^*} be the neighborhood around x^* with $|\mathcal{N}_{x^*}| = m$, and let $m' < m$ be an integer denoting the size of each bootstrap sample.

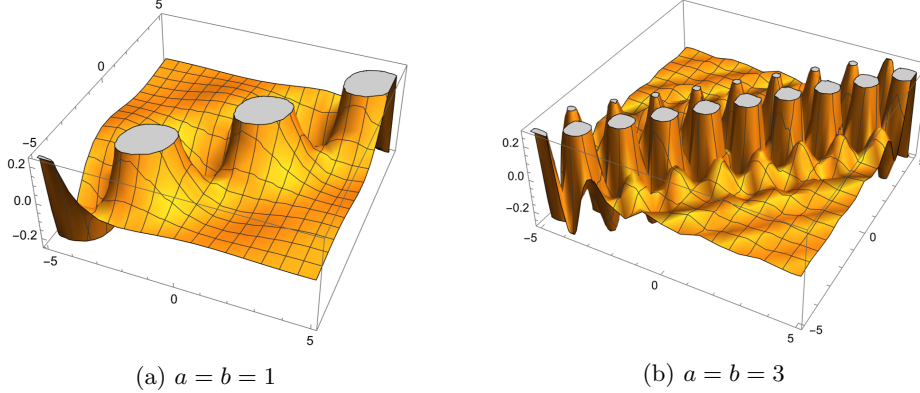


Figure 1: Ground truth model for our simulation study, defined in (5).

1. For some $c \in (0, 1)$, draw a sample of size $m' = \lfloor cm \rfloor$ uniformly at random from \mathcal{N}_{x^*} , creating the sub-neighborhood $\mathcal{N}'_{x^*} \subset \mathcal{N}_{x^*}$.
2. Fit a degree- k polynomial to $\{(z, f(z)) : z \in \mathcal{N}'_{x^*}\} \subset \mathcal{D}$, and record the estimated feature importance scores.
3. Repeat Steps 1 and 2 many times (e.g., 1,000), recording the feature importance scores obtained at every iteration.
4. For each $j \in [d]$, return the uncertainty interval $[L_j, U_j]$ where L_j and U_j are, respectively, the $(100 \cdot \frac{\alpha}{2})^{\text{th}}$ and $(100 \cdot (1 - \frac{\alpha}{2}))^{\text{th}}$ percentiles of the bootstrapped feature importance scores for feature j .

Time Complexity The complexity of constructing the explanation itself (Algorithm 1) is $O(dn + n \log n + mq^2 + q^3)$ using un-weighted regression, where q is the number of covariates used to fit the polynomial model g (which depends on its degree k , whether interaction terms are included, how the categorical features are encoded, etc.). The $dn + n \log n$ term is due to the computations for \mathcal{N}_{x^*} , assuming that sorting takes $O(n \log n)$ time and that $\pi_{x^*}(\cdot)$ can be computed in $O(d)$ time. Fitting the local polynomial requires $O(mq^2 + q^3)$ time, which can be straightforwardly obtained using the well-known facts that (i) the complexity of a standard matrix product AB , where $A \in \mathbb{R}^{a \times b}$, $B \in \mathbb{R}^{b \times c}$, is $O(abc)$; and (ii) the complexity of matrix inversion A^{-1} , where $A \in \mathbb{R}^{a \times a}$, is $O(a^3)$. If weighted regression is used, the resulting complexity is $O(dn + n \log n + m^2q + mq^2 + q^3)$. The complexities of the non-weighted and weighted versions of our bootstrap algorithm (Algorithm 2) can be determined in a similar manner and are given by $O(dn + n \log n + B(m'q^2 + q^3))$ and $O(dn + n \log n + B(m'^2q + m'q^2 + q^3))$, respectively.

4 Simulation Study

In this section, we demonstrate through Monte Carlo simulations that our non-parametric bootstrap method outperforms the naive theoretical confidence intervals from classical regression analysis. Specifically, we show that our approach attains a more favorable Pareto frontier representing the trade-off between interval width and coverage probability.

4.1 Naive Confidence Intervals

To obtain confidence intervals for our explanations, one could naively assume that the sampling distribution of the estimated feature importance scores is asymptotically a Gaussian distribution centered around the true importance scores. This is true if one is estimating partial derivatives using local polynomial regression and if the following assumptions from classical regression analysis hold: (i) The model is well-specified (it locally matches the true underlying model). (ii) Any error in the fit is due to mean-zero, i.i.d. Gaussian noise. In this case, the confidence interval of the importance score at confidence level $100 \times (1 - \alpha)\%$ is given by the

closed-form expression

$$\left[\hat{\theta} - z^* \cdot \text{se}(\hat{\theta}), \quad \hat{\theta} + z^* \cdot \text{se}(\hat{\theta}) \right]. \quad (1)$$

Here, $\hat{\theta}$ is the point estimator of the partial derivative, z^* is the z-score corresponding to confidence level $100 \times (1 - \alpha)\%$, and $\text{se}(\hat{\theta})$ is the standard error of the sampling distribution. For example, if a 95% confidence level is desired, the resulting bounds are $\hat{\theta} \pm 1.96 \times \text{se}(\hat{\theta})$.

Since the local polynomial model is linear in the regression coefficients, it follows that the partial derivative of the model with respect to any feature is also linear in the coefficients. Hence, $\text{se}(\hat{\theta}) \triangleq \sqrt{\text{Var}(\hat{\theta})}$ can be determined by computing the variance of a linear combination of the regression coefficients as follows. For simplicity, we consider the one-dimensional case and note that the derivation extends straightforwardly to the case of multiple covariates. Let g be the local polynomial model used in our explanation, which can be expressed as $g(x) = \sum_{\ell=0}^k \hat{\beta}_\ell \cdot x^\ell$. Then the estimated feature importance score is given by $\hat{\theta} = g'(x) = \hat{\beta}^\top v$, where $\hat{\beta} = [\hat{\beta}_1 \quad \hat{\beta}_2 \quad \dots \quad \hat{\beta}_k]^\top$ and $v \in \mathbb{R}^k$ is a vector with $v_\ell = \ell \cdot x^{\ell-1}$, $\ell \in \{1, 2, \dots, k\}$. It follows that

$$\text{Var}(\hat{\theta}) = \text{Var}(\hat{\beta}^\top v) = v^\top \Sigma v, \quad (2)$$

where $\Sigma \in \mathbb{R}^{k \times k}$ is the variance-covariance matrix of regression coefficients, such that $\Sigma_{ij} = \text{Cov}(\hat{\beta}_i, \hat{\beta}_j)$ for $i, j \in \{1, \dots, k\}$. In the case of the least squares estimator, we have

$$\hat{\beta} = (X^\top X)^{-1} X^\top y, \quad \Sigma = (X^\top X)^{-1} \sigma^2, \quad (3)$$

where σ^2 (the noise variance) can be estimated as

$$\hat{\sigma}^2 = \frac{1}{m - d - 1} \sum_{z \in \mathcal{N}_{x^*}} \left(f(z) - g(z) \right)^2. \quad (4)$$

4.2 Simulation Results

As a ground truth model, we use the function

$$S(x_1, x_2, a, b) = \sin(ax_1) \cos(bx_2) \tan\left(\frac{1}{1 + (x_1 - x_2)^2}\right), \quad (5)$$

where $x_1, x_2 \in [-5, 5]$ are continuous features and $a, b \in \{1, 2, 3\}$ are categorical features. The model is depicted for two different values of a and b in Figure 1. This function captures several complex characteristics often found in real-world ML models: it is not defined everywhere, approaches infinity in some regions, and is drastically sensitive to changes in the categorical values.

As a proof of concept, Figure 2 compares our method to the naive confidence intervals (using a significance level of .05 in both cases) at a randomly selected instance in the simulated data. The plot shows that our bootstrap interval captures the true feature importance scores for all of the features, whereas the naive confidence interval is too narrow for all but one of the features (x_1). Of course, in this particular example, one could achieve comparable performance with the naive intervals simply by “stretching” them (e.g., using a 99% confidence level to increase their width). Thus, it does not make sense to compare interval widths without controlling for coverage rate, and vice versa.

To ensure a proper comparison between the naive and bootstrap intervals, we analyze each method’s “Pareto frontier” for variable x_1 of the ground truth model. Specifically, we vary m , m' and k , and for each parameter set, we sample p points from the function (5). Using those p samples, we compute the average interval width and the empirical coverage probability for both the naive confidence interval and our bootstrap uncertainty interval. This yields two sets of tuples—one set corresponding to the naive intervals, the other to the bootstrap—of the form (Average Interval Width, Coverage Rate). To visualize the Pareto frontier, we plot these points in the two-dimensional plane as shown in Figure 3.

Figure 3 shows that our bootstrap method weakly dominates the naive theoretical intervals. For low coverage rates, the naive intervals and the bootstrap intervals exhibit the same trade-off between coverage rate and average interval width. However, around a coverage rate of 0.8, the naive intervals begin expanding

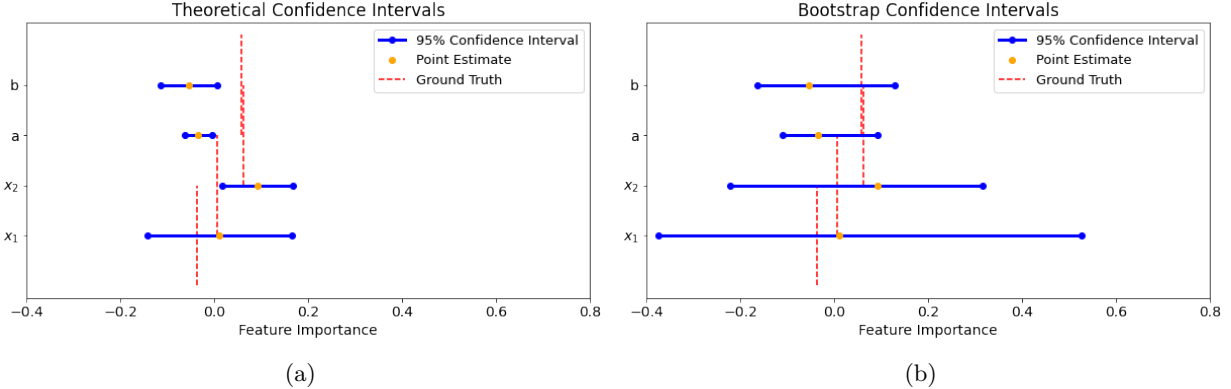


Figure 2: Comparison between the theoretical and bootstrap intervals using a synthetic dataset of size $n = 2,000$ sampled uniformly from the domain. To construct the explanations, we standardized the continuous features and one-hot encoded the categorical features, then fit a polynomial of degree $k = 4$ using weighted least squares regression with the $m = 66$ closest points. For the confidence intervals, we drew $B = 500$ bootstrap samples of size $m' = 59$, sampled uniformly from the neighborhood of $m = 66$ points.

with little gain in coverage rate, whereas the bootstrap method continues to increase its coverage rate as the interval widens. The intuition behind this result is two-fold. First, our bootstrap intervals are not centered around the point estimate, which allows them to have a higher coverage rate for a given interval width. Second, both methods have higher coverage rates when the local neighborhood is of moderate size but the polynomial degree is relatively high. This means that the naive approach has very few degrees of freedom, resulting in intervals that are not wide enough to cover the true parameter unless the point estimate is sufficiently close to the ground truth.

4.3 Choosing Hyperparameters

Figure 3 also provides important guidance on how to choose hyperparameters. Since, in general, the points lie on the Pareto frontier (aberrations are likely due to noise in the Monte Carlo procedure), a practitioner can specify a desired average interval width and set the hyperparameters to meet such a specification. While it would be impossible to know the coverage rate without a ground truth, the fact that all points lie on the Pareto frontier guarantee that no choice of hyperparameters is inefficient. That is, for a given choice of hyperparameters yielding a particular average interval width, there is not another set of hyperparameters yielding the same interval width with a higher coverage rate.

Figure 4 shows how to adjust the hyperparameters to achieve a desired interval width. Generally speaking, increasing m' decreases the interval width, as illustrated by the downward tendency of the points. Increasing m also decreases the interval width, as illustrated by the higher positioning of the blue points compared to the orange points. Finally, increasing k increases the interval width, as illustrated by the higher positioning of the \times marks compared to the \circ marks. These patterns make intuitive sense: the larger the fraction of points c used to compute the intervals, the higher the “overlap” between the bootstrap samples and thus the smaller the resulting interval width. The larger the local neighborhood (m), the less likely it is that the polynomial model captures the true ML model over the entire region; and if the true model varies significantly more than the flexibility of the polynomial allows, the polynomial coefficients will attenuate toward 0 and the resulting bootstrap interval width will decrease.⁵ Finally, higher-degree polynomials exhibit higher variance and have fewer degrees of freedom; thus, the bootstrap distribution is wider for larger k .

⁵To further drive home this intuition, suppose the true underlying model is a sine wave and the local polynomial is a line. The sine can be well-approximated by the line over small intervals (e.g., less than a quarter-period). However, as the interval expands, the approximation worsens and the fitted polynomial converges to a horizontal line (assuming un-weighted regression is performed). This intuition roughly extends to our ground-truth model (5), which exhibits similar periodic behavior, as illustrated in Figure 1.

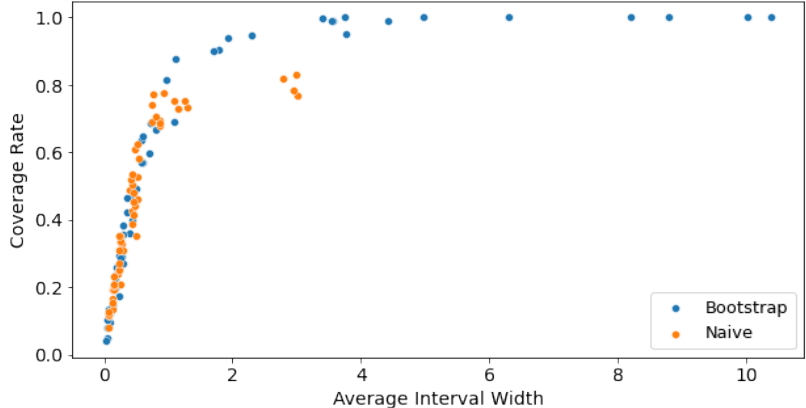


Figure 3: Comparison of the Pareto frontiers of the naive and bootstrap uncertainty intervals. The figure was generated by sweeping over all combinations of $k \in \{1, 2, 3, 4\}$, $m \in \{32, 64, 128, 256\}$, and setting m' such that $m' = \lfloor cm \rfloor$ with $c \in \{.3, .5, .7, .9\}$. Throughout, $n = 2,000$ and $p = 250$, but qualitatively similar results held for $n \in \{1000, 2000, 3000, 4000, 5000\}$.

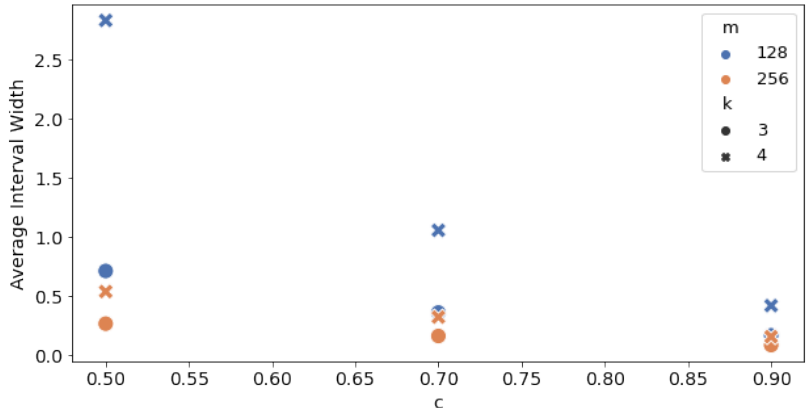


Figure 4: Average width of bootstrap uncertainty intervals as a function of m, k, c . The figure was generated by setting $n = 2,000$ and $p = 250$, but qualitatively similar results held for $n \in \{1000, 2000, 3000, 4000, 5000\}$.

4.4 Comparison with BayesLIME

BayesLIME [30] is an existing method for quantifying the uncertainty of model-agnostic explanations. In this section, we compare our bootstrap-based explanations and uncertainty measures with those of BayesLIME. We emphasize, however, that the environment for which BayesLIME was developed is different from ours in that BayesLIME assumes access to the underlying machine learning model and the ability to take an arbitrarily large number of samples from it. This inhibits a perfect apples-to-apples comparison between our bootstrap method and BayesLIME. However, we take the following measures to increase the fairness of the comparison: (i) We adapt BayesLIME to only leverage samples from the same fixed dataset available to our bootstrap method. (ii) To ensure that BayesLIME is not handicapped by its assumption of linearity, we endow BayesLIME with the ability to fit higher-order polynomials. The purpose of this exercise is not to show that our bootstrap method is unambiguously better than BayesLIME, but instead to show that when the assumption of model access is loosened, the leading methods that rely on model access may no longer be appropriate.

Figure 5 once again plots the Pareto frontier representing the trade-off between interval width and coverage rate. As in the case of the naive uncertainty intervals (Figure 3), BayesLIME does not achieve a coverage rate above 0.8—unless the intervals are made impractically large. While there may be intermediate parameter

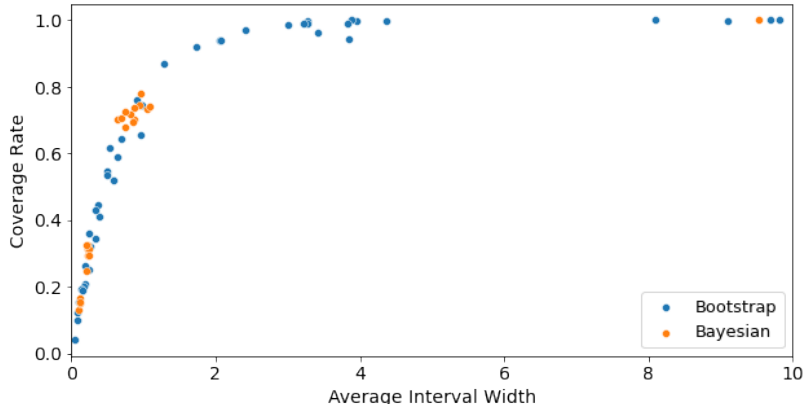


Figure 5: Comparison of the Pareto frontiers of the BayesLIME and bootstrap uncertainty intervals. The figure was generated by sweeping over all combinations of $k \in \{2, 3, 4\}$, $m \in \{64, 128, 256\}$, and setting m' such that $m' = \lfloor cm \rfloor$ with $c \in \{.3, .5, .7, .9\}$. Throughout, $n = 2,000$ and $p = 250$, but qualitatively similar results held for $n \in \{1000, 2000, 4000, 5000\}$.

sets in which BayesLIME achieves a coverage rate greater than 0.8, its greater sensitivity to hyperparameter selection inhibits its practicality. On the other hand, our bootstrap method traces a relatively smooth curve through the space and enables practitioners to better fine-tune their desired interval width. This provides evidence that without model access, our bootstrap method can achieve higher coverage rates than BayesLIME with more flexibility in setting the hyperparameters.

5 Real Data Experiments

We further demonstrate the capabilities of our method by applying it to two well-known tabular datasets: the German Credit dataset from the UCI machine learning repository [12] and the COMPAS recidivism dataset [6]. For each dataset, we trained a random forest classifier with 100 estimators on a random 80-20 train-test split. We treated the resulting classifier as a black-box model and collected its predictions on the entire dataset to form our historical dataset of model inputs and outputs. Due to the step-function-like behavior of the random forest models, we estimate the function differences with our bootstrap method instead of the partial derivatives. Additionally, before performing polynomial regression, we standardize the continuous features, one-hot encode the categorical features, and transform the response (i.e., the probabilities predicted by the model) to log-odds. (However, we convert log-odds back to probabilities when estimating the feature importance scores and uncertainty intervals.) We generated an explanation of model behavior for every instance in the test set and computed the following quantities for each feature: (i) the average absolute feature importance score (i.e., the magnitude of the estimated importance assigned to each feature, averaged over all test instances); and (ii) the average width of the bootstrap uncertainty intervals.

Figure 6 plots the resulting (**width**, **importance**) tuples for each feature. These plots provide a high-level view of the average influence of each feature on the model’s predictions, along with the corresponding uncertainty that arises from using a finite sample to estimate these quantities. For example, Figure 6a shows that the **Priors Count** and **Sex** features have a high average importance but are also accompanied by high uncertainty. On the other hand, **Length of Stay** has a lower average importance but also lower uncertainty. Finally, the **Race** feature has a relatively high average importance along with a moderate level of uncertainty. Conclusions can be drawn from Figure 6b in a similar fashion. We see that the **OtherLoansAtBank** and **Unemployed** features have both high average importance and low uncertainty, whereas **LoanDuration** and **LoanAmount** have higher uncertainty, and **HasTelephone** has both low average importance and low uncertainty. In practice, after making such observations, one might further investigate the model for issues related to bias and fairness, or attempt to improve the fidelity of the explanation by collecting more data based on the highest-uncertainty features.

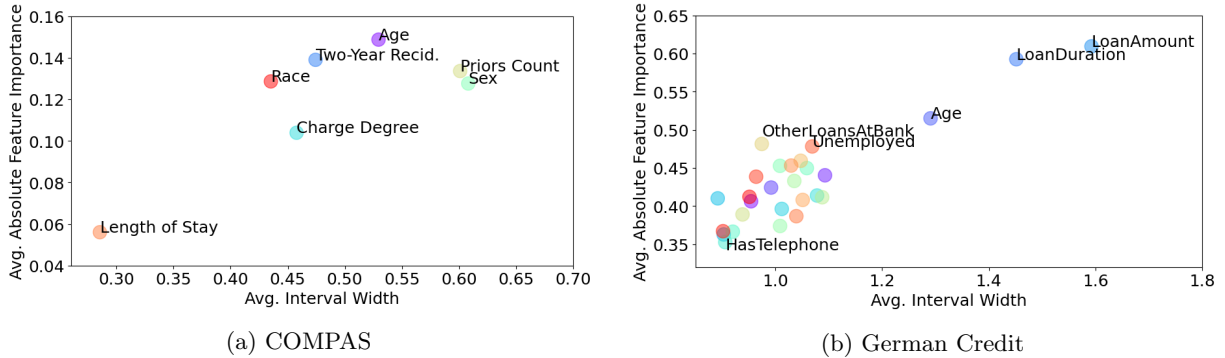


Figure 6: Visual summary of feature importance scores and corresponding uncertainty measures for two different datasets.

6 Conclusions and Future Work

We developed a method for generating local explanations from a fixed dataset of model queries, obviating the need for direct model access. We also developed a non-parametric bootstrapping technique for quantifying the uncertainty in our explanations, motivated by the fact that our setting does not fit neatly into the standard statistical estimation paradigm. Through simulation studies, we showed that our bootstrap confidence intervals outperform (i) a theoretical approach from frequentist statistics that makes strong distributional assumptions about the estimated feature importance scores; and (ii) a Bayesian method for quantifying the uncertainty in explanations [30]. Lastly, we applied our method to two real datasets and demonstrated its ability to simultaneously yield insights into the behavior of the black-box model as well as the inherent uncertainty of our explanations due to the fixed nature of the query data.

Future directions include extending our method to other data modalities such as text and images; investigating its performance using other bootstrap methods, such as bias-corrected and accelerated (BCa) bootstrap; and studying an “active learning” variant of our problem in which we can further query the model after observing the initial explanations and uncertainty intervals. Finally, we seek to explore alternative frameworks, which are fundamentally different from the statistical approach taken in this paper, such as approximation theory [10].

References

- [1] Amina Adadi and Mohammed Berrada. Peeking inside the black-box: a survey on explainable artificial intelligence (XAI). *IEEE Access*, 6:52138–52160, 2018.
- [2] Chirag Agarwal, Nari Johnson, Martin Pawelczyk, Satyapriya Krishna, Eshika Saxena, Marinka Zitnik, and Himabindu Lakkaraju. Rethinking stability for attribution-based explanations. *arXiv preprint arXiv:2203.06877*, 2022.
- [3] Chirag Agarwal, Marinka Zitnik, and Himabindu Lakkaraju. Probing GNN explainers: A rigorous theoretical and empirical analysis of GNN explanation methods. In *International Conference on Artificial Intelligence and Statistics*, pages 8969–8996. PMLR, 2022.
- [4] David Alvarez-Melis and Tommi S Jaakkola. On the robustness of interpretability methods. *arXiv preprint arXiv:1806.08049*, 2018.
- [5] Marco Ancona, Enea Ceolini, Cengiz Öztireli, and Markus Gross. Gradient-based attribution methods. In *Explainable AI: Interpreting, Explaining and Visualizing Deep Learning*, pages 169–191. Springer, 2019.
- [6] Julia Angwin, Jeff Larson, Surya Mattu, and Lauren Kirchner. Machine bias. In *Ethics of Data and Analytics*, pages 254–264. Auerbach Publications, 2016.

- [7] David Baehrens, Timon Schroeter, Stefan Harmeling, Motoaki Kawanabe, Katja Hansen, and Klaus-Robert Müller. How to explain individual classification decisions. *The Journal of Machine Learning Research*, 11:1803–1831, 2010.
- [8] Jonathan W Bartlett and Rachael A Hughes. Bootstrap inference for multiple imputation under uncongeniality and misspecification. *Statistical methods in medical research*, 29(12):3533–3546, 2020.
- [9] Philippe Bracke, Anupam Datta, Carsten Jung, and Shayak Sen. Machine learning explainability in finance: an application to default risk analysis. 2019.
- [10] Elliott Ward Cheney and William Allan Light. *A course in approximation theory*, volume 101. American Mathematical Soc., 2009.
- [11] Filip Karlo Došilović, Mario Brčić, and Nikica Hlupić. Explainable artificial intelligence: A survey. In *2018 41st International Convention on Information and Communication Technology, Electronics and Microelectronics (MIPRO)*, pages 0210–0215. IEEE, 2018.
- [12] Dheeru Dua, Casey Graff, et al. UCI machine learning repository. 2017.
- [13] Bradley Efron. Bootstrap methods: Another look at the jackknife. In *Breakthroughs in Statistics*, pages 569–593. Springer, 1992.
- [14] Bradley Efron and Robert J Tibshirani. *An Introduction to the Bootstrap*. CRC press, 1994.
- [15] Leilani H. Gilpin, Vishnu Penubarthi, and Lalana Kagal. Explaining multimodal errors in autonomous vehicles. In *2021 IEEE 8th International Conference on Data Science and Advanced Analytics (DSAA)*, pages 1–10, 2021.
- [16] Bryce Goodman and Seth Flaxman. European union regulations on algorithmic decision-making and a “right to explanation”. *AI Magazine*, 38(3):50–57, 2017.
- [17] Mehmet A Gulum, Christopher M Trombley, and Mehmed Kantardzic. A review of explainable deep learning cancer detection models in medical imaging. *Applied Sciences*, 11(10):4573, 2021.
- [18] Giacomo Iadarola, Fabio Martinelli, Francesco Mercaldo, and Antonella Santone. Towards an interpretable deep learning model for mobile malware detection and family identification. *Computers & Security*, 105:102198, 2021.
- [19] Dong-sup Kim and Seungwoo Shin. The economic explainability of machine learning and standard econometric models-an application to the US mortgage default risk. *International Journal of Strategic Property Management*, 25(5):396–412, 2021.
- [20] Pantelis Linardatos, Vasilis Papastefanopoulos, and Sotiris Kotsiantis. Explainable AI: A review of machine learning interpretability methods. *Entropy*, 23(1):18, 2020.
- [21] Saskia Litière, Ariel Alonso, and Geert Molenberghs. Type I and type II error under random-effects misspecification in generalized linear mixed models. *Biometrics*, 63(4):1038–1044, 2007.
- [22] Scott M Lundberg and Su-In Lee. A unified approach to interpreting model predictions. *Advances in Neural Information Processing Systems*, 30, 2017.
- [23] Sina Mohseni, Niloofar Zarei, and Eric D Ragan. A multidisciplinary survey and framework for design and evaluation of explainable AI systems. *ACM Transactions on Interactive Intelligent Systems (TiiS)*, 11(3-4):1–45, 2021.
- [24] Harsha Nori, Samuel Jenkins, Paul Koch, and Rich Caruana. InterpretML: A unified framework for machine learning interpretability. *arXiv preprint arXiv:1909.09223*, 2019.
- [25] Marco Tulio Ribeiro, Sameer Singh, and Carlos Guestrin. “Why should I trust you?” Explaining the predictions of any classifier. In *Proceedings of the 22nd ACM SIGKDD International Conference on Knowledge Discovery and Data Mining*, pages 1135–1144, 2016.

- [26] Mark O Riedl. Human-centered artificial intelligence and machine learning. *Human Behavior and Emerging Technologies*, 1(1):33–36, 2019.
- [27] Jonas Schulz, Rafael Poyiadzi, and Raul Santos-Rodriguez. Uncertainty quantification of surrogate explanations: an ordinal consensus approach. *arXiv preprint arXiv:2111.09121*, 2021.
- [28] Joshua Silver and Tate Huffman. Baseball predictions and strategies using explainable AI. In *The 15th Annual MIT Sloan Sports Analytics Conference*, 2021.
- [29] Karen Simonyan, Andrea Vedaldi, and Andrew Zisserman. Deep inside convolutional networks: Visualising image classification models and saliency maps. *arXiv preprint arXiv:1312.6034*, 2013.
- [30] Dylan Slack, Anna Hilgard, Sameer Singh, and Himabindu Lakkaraju. Reliable post hoc explanations: Modeling uncertainty in explainability. *Advances in Neural Information Processing Systems*, 34:9391–9404, 2021.
- [31] Daniel Smilkov, Nikhil Thorat, Been Kim, Fernanda Viégas, and Martin Wattenberg. Smoothgrad: removing noise by adding noise. *arXiv preprint arXiv:1706.03825*, 2017.
- [32] Jost Tobias Springenberg, Alexey Dosovitskiy, Thomas Brox, and Martin Riedmiller. Striving for simplicity: The all convolutional net. *arXiv preprint arXiv:1412.6806*, 2014.
- [33] The White House Office of Science and Technology Policy. Blueprint for an AI bill of rights, Oct 2022. Accessed: 2022-10-24.
- [34] Stijn Vansteelandt, Maarten Bekaert, and Gerda Claeskens. On model selection and model misspecification in causal inference. *Statistical methods in medical research*, 21(1):7–30, 2012.
- [35] Kristoffer Wickstrøm, Karl Øyvind Mikalsen, Michael Kampffmeyer, Arthur Revhaug, and Robert Jenssen. Uncertainty-aware deep ensembles for reliable and explainable predictions of clinical time series. *IEEE Journal of Biomedical and Health Informatics*, 25(7):2435–2444, 2020.
- [36] Benjamin Wilson, Judy Hoffman, and Jamie Morgenstern. Predictive inequity in object detection. *arXiv preprint arXiv:1902.11097*, 2019.
- [37] Feiyu Xu, Hans Uszkoreit, Yangzhou Du, Wei Fan, Dongyan Zhao, and Jun Zhu. Explainable AI: A brief survey on history, research areas, approaches and challenges. In *CCF International Conference on Natural Language Processing and Chinese Computing*, pages 563–574. Springer, 2019.
- [38] Yujia Zhang, Kuangyan Song, Yiming Sun, Sarah Tan, and Madeleine Udell. “Why should you trust my explanation?” Understanding uncertainty in LIME explanations. *arXiv preprint arXiv:1904.12991*, 2019.